Journal of Orthopaedic Translation 37 (2022) 152–162

Contents lists available at ScienceDirect

Journal of Orthopaedic Translation

journal homepage: www.journals.elsevier.com/journal-of-orthopaedic-translation

Bone tissue engineering scaffolds with HUVECs/hBMSCs cocultured on 3D-printed composite bioactive ceramic scaffolds promoted osteogenesis/angiogenesis

Xiao Liu [a,1], Naru Zhao [c,f,1], Haifeng Liang [d], Bizhi Tan [a,h], Fangli Huang [a], Hao Hu [a], Yan Chen [a], Gang Wang [a], Zemin Ling [a], Chun Liu [a,e], Yali Miao [b,g,*], Yingjun Wang [c,f,**], Xuenong Zou [a,***]

[a] Guangdong Provincial Key Laboratory of Orthopaedics and Traumatology, Department of Spine Surgery, The First Affiliated Hospital of Sun Yat-sen University, Guangzhou, 510080, China
[b] Department of Orthopedics, Guangdong Provincial People's Hospital, Guangdong Academy of Medical Sciences, Guangzhou, 510080, China
[c] National Engineering Research Center for Tissue Restoration and Reconstruction, Guangzhou, China
[d] Department of Orthopedics, Zhujiang Hospital, Southern Medical University, No. 253 Industrial Avenue, Haizhu, Guangzhou, 510280, China
[e] Center for Translational Medicine, Precision Medicine Institute, The First Affiliated Hospital of Sun Yat-sen University, Guangzhou, China
[f] School of Materials Science and Engineering, South China University of Technology, Guangzhou, 510641, China
[g] Guangdong Cardiovascular Institute, Guangdong Provincial People's Hospital , Guangdong Academy of Medical Sciences, Guangzhou, Guangdong, China
[h] Department of Orthopaedics, Sun Yat-Sen Memorial Hospital, Sun Yat-Sen University, Guangzhou, 510120, China

ARTICLE INFO

Keywords:
Bioactive ceramic scaffolds
3D printing
HUVECs/hBMSCs coculture
Bone tissue engineering scaffolds
Real-time cell tracking

ABSTRACT

Background: /Objective: Tissue engineering involves scaffolds, cells and growth factors, among which growth factors have limited applications due to potential safety risks and high costs. Therefore, an alternative approach to exogenously induce osteogenesis is desirable. Considering that osteogenesis and angiogenesis are coupled, a system of human umbilical vein endothelial cells (HUVECs) and human bone mesenchymal stem cells (hBMSCs) coculture is more biologically adapted to the microenvironment *in vivo* and can mediate osteogenesis and angiogenesis *via* paracrine signalling. Hence, in this study, a HUVECs/hBMSCs coculture system with appropriate cell and medium proportions was established. The substrate for the coculture system was a 3D-printed composite bioceramic scaffold (β-TCP/$CaSiO_3$) based on a previous study. The aim of this study was to explore the potential of this system for bone tissue engineering.

Methods: Bioactive ceramic scaffolds for tissue engineering were fabricated *via* a 3D Bioplotter™ system. The coculture system for *in vitro* and *in vivo* studies consisted of direct contact between HUVECs and hBMSCs cultured on the 3D-printed scaffolds.

Results: The proportions of HUVECs/hBMSCs and medium components were determined by cell viability, and the coculture system showed negligible cytotoxicity. CD31 secreted by HUVECs formed strings, and cells tended to aggregate in island chain-like arrays. Real-time cell tracking showed that HUVECs were recruited by hBMSCs, and the integrin expression by HUVECs was upregulated. Ultimately, osteogenic and angiogenic marker gene expression and protein secretion were upregulated. Moreover, the obtained bone tissue engineering scaffolds could induce early osteogenic protein secretion and capillary tube formation in nude rats.

Conclusion: These bone tissue engineering scaffolds without exogenous growth factors exhibited the ability to promote osteogenesis/angiogenesis.

Translational potential of this article: The fabricated 3D-printed bioactive ceramic scaffolds could provide mechanical, biodegradable and bioadaptive support for personalized bone regeneration. In addition, the bone tissue

* Corresponding author. Department of Orthopedics, Guangdong Provincial People's Hospital, Guangdong Academy of Medical Sciences, Guangzhou, 510080, China.
** Corresponding author. National Engineering Research Center for Tissue Restoration and Reconstruction, Guangzhou, China.
*** Corresponding author.
E-mail addresses: liux539@mail.sysu.edu.cn (X. Liu), nrzhao@scut.edu.cn (N. Zhao), 397957332@qq.com (H. Liang), tbzhi@outlook.com (B. Tan), huangfli@mail2.sysu.edu.cn (F. Huang), huhao7@mail2.sysu.edu.cn (H. Hu), cheny585@mail2.sysu.edu.cn (Y. Chen), 451694101@qq.com (G. Wang), lingzm3@mail.sysu.edu.cn (Z. Ling), liuch393@sysu.edu.cn (C. Liu), miaoyali@gdph.org.cn (Y. Miao), imwangyj@163.com (Y. Wang), zouxuen@mail.sysu.edu.cn (X. Zou).
[1] The author contributed equally to the work.

https://doi.org/10.1016/j.jot.2022.10.008
Received 22 April 2022; Received in revised form 30 September 2022; Accepted 12 October 2022

engineering scaffolds exhibited the ability to promote osteogenesis/angiogenesis without the addition of exogenous growth factors, thus mitigating safety risks. Although application of the HUVECs/hBMSCs coculture system might be a time-consuming process, further development of cord blood storage could be beneficial for multicell coculture.

1. Introduction

Bone repair is a complex and long process, and bone tissue engineering scaffolds with excellent osteogenesis/angiogenesis could be potential candidates for bone regeneration applications [1]. Growth factors can bind to specific receptors on target cells and efficiently stimulate cells [2]; however, growth factors are limited by high costs, potential side effects, production processes, dose control, high batch variability and species-related problems [3,4]. Considering microenvironment bioadaptability *in vivo*, suitable types of seed cells are compatible with the natural biological microenvironment [5,6]. Cell fate can be mediated by paracrine signalling [7], and secreted chemotactic factors can promote cell recruitment and gap junction formation [8]. As a result, cellular behaviours can be mediated to achieve bone regeneration.

Mesenchymal stem cells (MSCs) have the potential to differentiate into mesodermal cell types [9] and have been widely utilized in tissue engineering or as medicinal signalling cells [10]. MSCs can also supply exogenous factors that induce site- or tissue-specific resident stem cells to construct new tissue [11]. In addition, osteogenesis and angiogenesis are coupled since vessels provide nutrients and oxygen, remove waste [12] and maintain metabolism to balance homeostasis [13,14]. The paracrine signalling of vascular endothelial growth factor (VEGF) and bone morphogenetic protein 2 (BMP2) between human umbilical vein endothelial cells (HUVECs) and human bone mesenchymal stem cells (hBMSCs) has been reported to be a complementary factor in angiogenesis and osteogenesis [6]. Hence, HUVECs/hBMSCs coculture might promote osteogenesis and angiogenesis [15]. In this study, a coculture system with HUVECs and hBMSCs was utilized.

Various approaches are used for coculture [16]: direct contact includes 3D and 2D conditions, and indirect contact can be further divided into three approaches, namely, semipermeable membrane separation, conditioned medium and conditioned endothelial cell medium (ECM) [17,18]. Coculture with indirect contact is used to study the mechanism and relationships formed by paracrine signalling, while coculture with direct contact on scaffolds is used to study candidates for tissue engineering applications. In addition, 3D scaffolds with direct-contact coculture can be used to produce MSCs/HUVECs spheroids, which are crucial for exosome secretion by MSCs [19–21]. Additionally, interconnected porosity has been proven to be necessary for an implant to induce osteogenesis [22]. 3D printing techniques have the inherent advantage of fabricating interconnected porous scaffolds [23,24] and could play an important role in personalized bone regeneration [25]. Therefore, 3D-printed interconnected porous bioactive ceramic scaffolds were utilized as the substrate for HUVECs/hBMSCs culture. In our previous studies, 3D-printed composite ceramic scaffolds were fabricated using $CaSiO_3$ [26], which promoted osteogenesis and angiogenesis [27], and the effects of the proportion of β-TCP/$CaSiO_3$ on MSCs were studied. In addition, the shape, size and porosity of the scaffolds were selected based on our previous study [28].

In this study, a coculture system consisting of HUVECs and hBMSCs was established on porous β-TCP/$CaSiO_3$ scaffolds fabricated by a 3D Bioplotter™ system (Regenovo, China). The direct coculture strategy was achieved via the successive seeding of HUVECs/hBMSCs onto the 3D printed scaffolds; then, the tissue engineering scaffolds were evaluated via *in vitro* and *in vivo* studies, the process was showed in Scheme 1. Cell and medium proportions were optimized based on cell viability assessments, and the established coculture system, which aimed to promote osteogenesis/angiogenesis, was also assessed via immunofluorescence and *in vitro* real-time tracking (0–48 h). After HUVECs/hBMSCs were cocultured on β-TCP/$CaSiO_3$ 3D printed scaffolds, the expression of genes and the secretion of proteins related to osteogenesis and angiogenesis were detected *in vitro*. For the *in vivo* study, nude rats were utilized to avoid an immune rejection response, and the extent of osteogenesis/angiogenesis after submuscular implantation was assessed to reveal the osteoinductive capacity of the bone tissue engineering scaffolds.

2. Materials and methods

HUVECs and ECM were purchased from Sciencell, USA. The ECM contained 5% fetal bovine serum (FBS, Catalogue No.0025), 1% endothelial growth additives (ECGS, Catalogue No.1052), and 1% penicillin streptomycin solution (P/S, Catalogue No.0503). HUVECs were primary cultured. hBMSCs (passage 2) and complete medium (HUXMA-90011) were purchased from Cyagen Biosciences, USA. Complete medium contained 10% FBS, 1% L-glutamine and 1% penicillin streptomycin solution.

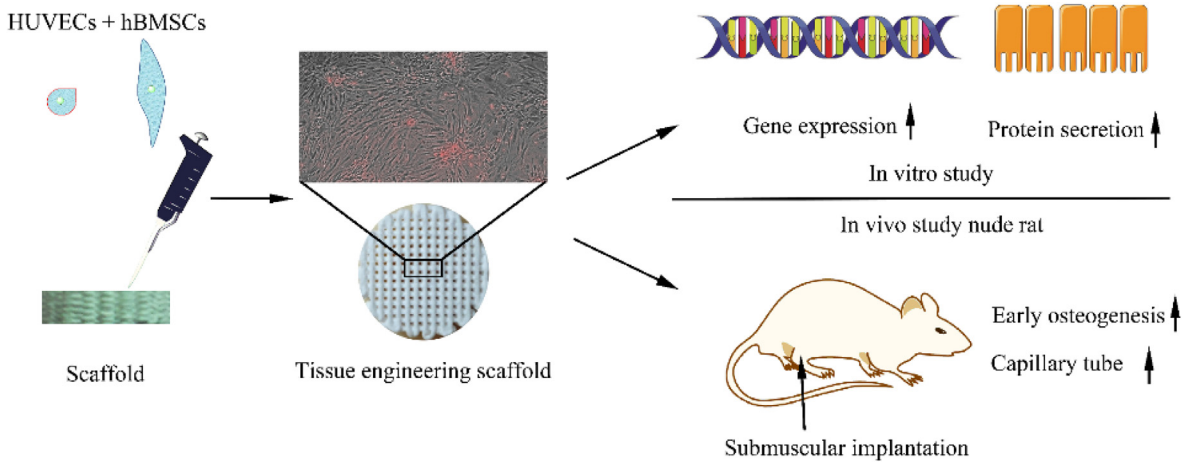

Scheme 1. Overview of the experiment. The HUVECs/hBMSCs were seeded onto the 3D printed scaffolds fabricated by a 3D Bioplotter™ system and the tissue engineering scaffolds were evaluated via *in vitro* and *in vivo* studies.

2.1. Scaffold fabrication

The scaffolds were fabricated based on our previous study [26]. Briefly, the raw materials, β-tricalcium phosphate and silicate calcium particles, were prepared by chemical precipitation. Ammonium polyacrylate (PAA-NH_4) and hydroxypropylmethyl cellulose (MV = 4000) were used as the dispersant and viscosifier, respectively. The dispersant and viscosifier were mixed the raw materials with a planetary ball mill (Nanda Instrument Plant, Nanjing, China). Ultimately, the slurry used for rapid prototyping was endowed with liquidity and the ability to solidify. An extrusion rapid prototyping 3D Bioplotter™ system (Regenovo, Hangzhou, China) was used for rapid prototyping. The printed scaffolds were sintered at 1100 °C.

2.2. Characterization of scaffolds

The morphology and exterior of the scaffolds were observed by field emission scanning electron microscopy (SEM) (Zeiss Merlin, Germany). Before SEM observation, the samples were sputter-coated with platinum, and an electroconductive paste was twined laterally to link the upper surface with the platform. X-ray diffraction (XRD) and energy dispersive spectroscopy (EDS) were utilized to measure the crystal phase and elements in the scaffolds.

2.3. Cell culture and seeding

HUVECs and hBMSCs were cultured separately in an incubator at 37 °C and with 5% CO_2 before seeding. HUVECs and hBMSCs were seeded at passages 3–5 and 4–6. The culture medium was prepared as specified and refreshed every 2 days. Trypsin solution with 0.25% EDTA was utilized to detach cells from the culture flask. The interval for seeding different cells was 6–8 h to ensure cells adhered to the substrate. The scaffolds used in the experiment were sterilized by autoclaving (121 °C, 30 min) and soaked in phosphate buffer for 12 h before seeding.

2.4. Viability of cocultured cells

Cell viability was evaluated for different ratios of cells and medium components. The CCK-8 (Dojindo, Kumamoto, Japan) assay was used to characterize the intracellular dehydrogenase density and assess cell viability after 24 and 48 h of coculture. HUVECs and hBMSCs at ratios of 0:1, 1:2, 1:1, 2:1 and 1:0 were cocultured in medium consisting of ECM and HUXMA at ratios of 0:1, 1:2, 1:1, 2:1 and 1:0, respectively. CCK-8 working solution (330 μL) containing a 10:1 ratio of medium and stock solution was added to each well. Then, the plate was incubated for 1 h before analysis with a microplate reader at a wavelength of 450 nm. The cytotoxicity of the coculture system was assessed by detecting the concentration of lactate dehydrogenase, which was released only by damaged cells.

2.5. Cell adhesion

Cell adhesion on scaffolds was quantified and characterized by measuring the expression of the integrin subunits α_2, α_5, α_v and β_1 in the early stage (12 h) via real-time polymerase chain reaction (RT–PCR) analysis. The combinations of the subunits were listed below in Table 1. Before extracting RNA, Dynabeads (Dynabeads™ CD31 Endothelial Cell 11155D, Life, USA) were utilized to isolate cells. Dynabeads bind to CD31 receptors on target cells, allowing the cells to be separated under a magnetic field. The process of RT–PCR was as follows [29]. ***(1) DNA extraction.*** TRIzol was used to lyse cells, chloroform was used to split the water from the oil phase, and isopropanol was used to precipitate RNA. ***(2) Reverse transcription.*** The obtained RNA was quantified by a NanoDrop2000 spectrophotometer (Thermo Scientific, USA) and then normalized according to the manufacturer's protocol for the reverse transcription assay. The extracted RNA was reverse transcribed into cDNA using a PrimeScript RT reagent kit with gDNA Eraser (TaKaRa Biotechnology, Japan). ***(3) Characterization.*** The cDNA was analysed with QuantStudio 6 Flex RT-PCR system software (Applied Biosystems, USA), and quantitative polymerase chain reaction (qPCR) was performed with a SYBR green assay (Iq Supermix, Bio-Rad). The housekeeping gene was GAPDH, and the primers for the integrin subunits α_2, α_5, α_v and β_1 were listed in Table 2. Gene expression was compared by $\triangle\triangle$Ct analysis, where Ct represented the cycle time after the threshold was reached.

Qualitative observation was performed by SEM. Firstly, cells were fixed in 2.5% glutaraldehyde for more than 12 h after cultured on scaffolds for 3 d. Secondly, dehydration was performed as follows with an alcohol gradient treatment: glutaraldehyde was removed from each well; phosphate-buffered saline was used to wash the scaffolds three times; scaffolds were treated with 50%, 70%, 80%, 90%, 95% and 100% alcohol for 60 min, 30 min, 20 min, 10 min, 5 min and 5 min, respectively, in sequence. Finally, the samples were dried in an oven and then coated with Pt for observation.

2.6. Real-time cell tracking in vitro

To distinguish the cell distribution by optical observation, the cell dye CM-Dil (C7001, Life, USA) and CellTracker Green CMFDA dye (C7025, Life, USA) were used to label HUVECs and hBMSCs. CM-Dil was diluted with Dulbecco's phosphate-buffered saline, and the concentration of the working solution was 2.5 μg/mL 2 mL of CM-Dil solution was added to the HUVECs culture flask, and then the culture flask was incubated at room temperature for 5 min before being placed in a 4 °C refrigerator for 15 min. CellTracker Green CMFDA dye at a concentration of 5 μg/mL was reacted with hBMSCs in the culture flask for 30 min at room temperature. Then, the samples were observed by laser scanning confocal microscopy (Leica TCS SP8, Germany).

2.7. Osteogenic and angiogenic gene expression

The expression levels of osteogenic and angiogenic genes were characterized by RT-PCR using the same process as that used for the analysis of integrin subunit expression. The housekeeping gene was GAPDH, and the osteogenic gene markers were the alpha 1 chain of type I collagen (Col-I), BMP2, osteocalcin (OCN) and osteopontin (OPN). The gene markers for angiogenesis were basic fibroblast growth factor (bFGF), platelet endothelial cell adhesion molecule (PECAM-1 or CD31), endothelial nitric oxide synthase (eNOS), kinase domain region receptor (KDR or VEGF-R2), transforming growth factor-β (TGF-β) and VEGF. The

Table 1
Vertebrate integrins [30].

Combination	Synonyms	Ligands
$\alpha_2\beta_1$	VLA-2	Collagens, laminins
$\alpha_5\beta_1$	VLA-5; fibronectin receptor	Fibronectin, proteinases
$\alpha_v\beta_1$		Vitronectin; fibrinogen

Table 2
Primer sequences for integrin RT-PCR.

Gene	Direction	Sequence (5′-3′)
GAPDH	Forward	TGTGTCCGTCGTGGATCTGA
	Reverse	TTGCTGTTGAAGTCGCAGGAG
α_2	Forward	CAAGAGGGGAAAACAAAACACA
	Reverse	CAGCCGTGGTCTAAAAGGAAC
α_5	Forward	CAAAGCCCTGAAGATGCCCTA
	Reverse	ATCCACAGTGGGACGCCATA
α_v	Forward	AAACTCGCCAGGTGGTATGTGA
	Reverse	CTGGTGCACACTGAAACGAAGA
β_1	Forward	GGTTTCACTTTGCTGGAGATGG
	Reverse	CAGTTTCTGGACAAGGTGAGCAATA

Table 3
Primer sequences for osteogenic and angiogenic genes.

Gene	Direction	Sequence (5′-3′)
GAPDH	Forward	TGTGTCCGTCGTGGATCTGA
	Reverse	TTGCTGTTGAAGTCGCAGGAG
BMP2	Forward	TGTGGAGGGTTGTGGGTGT GAA
	Reverse	TCAACTGGGGTGGGGTTTT
OPN	Forward	TGCAAACACCGTTGTAACCAAAAGC
	Reverse	TGCAGTGGCCGTTTGCATTTCT
OCN	Forward	AGCAGCTTGGCCCAGACCTA
	Reverse	TAGCGCCGGAGTCTGTTCACTAC
Col-I	Forward	GCTTGGTCCACTTGCTTGAAGA
	Reverse	GAGCATTGCCTTTGATTGCTGGTA
bFGF	Forward	GTGTGCTAACCGTTACCTGGCTATGCAAAAGC
	Reverse	CCAGTTCGTTTCAGTGCCACATTCT
CD31	Forward	CCGCATATCCAAGGTCAGCA
	Reverse	CACCTTGGTCCAGATGTGTGAA
eNOS	Forward	CTGAAGGCTGGCATCTGGAA
	Reverse	CATGTTACTGTGCGTCCACTCTG
KDR	Forward	AGCCAGCTCTGGATTTGTGGA
	Reverse	CATGCCCTTAGCCACTTGGAA
TGF-β	Forward	TCCTGGCGATACCTCAGCAA
	Reverse	GCTAAGGCGAAAGCCCTCAA
VEGF	Forward	CATCCAATCGAGACCCTGGTG
	Reverse	TTGGTGAGGTTTGATCCGCATA

primer sequences for the osteogenic and angiogenic genes were listed in Table 3.

2.8. Immunofluorescence

Protein secretion was detected by immunofluorescence using OCN and CD31 as markers. The primary CD31 antibody was a monoclonal CD31 antibody (JC/70A) (Life, USA) with a goat anti-mouse IgG (H+L) highly cross-adsorbed secondary antibody (Alexa Fluor 594, Life, USA). The primary antibody against OCN was a polyclonal rabbit antibody (23418-1-AP, Proteintech, Wuhan, China) with a donkey anti-rabbit IgG (H+L) secondary antibody conjugated with Alexa Fluor 647 (Life, USA). The processes were as follows. ***(1) Cell fixation***. 4% paraformaldehyde was added to each well, and then the plate was placed at 4 °C for more than 12 h ***(2) Cellular permeability***. After removing the paraformaldehyde, 1 mL of 0.1% Triton X-100 was utilized for 15 min ***(3) Sealing***. 1% bovine serum albumin in phosphate-buffered saline was used to prevent nonspecific adsorption. ***(4) Primary antibody***. Primary antibodies against CD31 and OCN were added to each well successively, and the incubation time ranged from 8 to 10 h ***(5) Secondary antibody***. Samples were then reacted with the corresponding secondary antibody at room temperature for 1 h ***(6) Staining***. Nuclei were stained with DAPI for 5 min.

2.9. In vivo surgery

Nude rats were used as an *in vivo* model for ectopic osteogenesis to avoid the immune problems caused by nonhomologous seed cells. After cells were cultured on the scaffolds for 1 week *in vitro*, the tissue engineering scaffolds were embedded into the biceps femoris (thigh muscle). The nude rats used for the experiment were female and weighed approximately 16–18 g. After the rats were anaesthetized, the rats were randomly divided into three groups, with a total of 30 nude rats. Implants were harvested at 2, 4 and 8 weeks, and both biceps femoris muscles of each nude rat received an implant. All protocols, surgical processes, aseptic operations and postoperative antibiotic treatments were performed according to relevant standards and regulations, and the surgical operations were approved by the Ethics Committee of Southern Medical University.

2.10. Pathology and histology

Harvested implants were fixed in 4% paraformaldehyde and decalcified with EDTA, followed by dehydration, permeation, wax saturation and embedding. Ultimately, implants were sectioned for haematoxylin-eosin (H&E) and Masson's trichrome staining to examine new bone matrix and collagen deposition. The expression of CD31 and OCN was characterized by immunohistochemical staining.

2.11. Statistical analysis

Experimental results are shown as means with standard deviations as error bars. Data were evaluated by one-way analysis of variance (ANOVA) followed by Tukey's test, with statistical significance set at $p < 0.05$ (marked as #).

3. Results

3.1. Scaffold morphology

The bioactive ceramic scaffolds were fabricated by the 3D Bioplotter™ system, as shown in Fig. 1A. The thermally treated scaffolds contained interconnected pores and micropores on the surface, as shown in Fig. 1B. The scaffolds for the *in vitro* experiments were 8-mm-diameter cylinders with a height of 2.5 mm (Fig. 1C). Fig. 1E showed the rectangular scaffold used for submuscular implantation. The crystal phase and elements of the scaffolds were measured via XRD and EDS. The surface layer consisted of β-TCP and $CaSiO_3$ (Fig. 1G). The circles correspond to the clear peak positions of β-TCP at 27.95° (131), 31.2° ($\overline{4}$ 22) and 34.6° (040). A peak at 30.06° corresponding to wollastonite (302) was also detected. The weights and atomic percentages of Ca, P and Si were shown in Fig. 1H.

3.2. Coculture system determination

The proportions of cells in the coculture system were selected by measuring cell viability. The number of cells was set as 6×10^4. The results were summarized in Fig. 2. The number of hBMSCs was 0 (red column), 2×10^5 (blue column), 3×10^5 (cyan column), 4×10^5 (pink column), and 6×10^5 (brown column), and the corresponding proportions of hBMSCs to HUVECs were 0:1 (0%), 1:2 (33%), 1:1 (50%), 2:1 (66%) and 1:0 (100%). The HUXMA contents were 0%, 33%, 50%, 66% and 100%, and the proportions of conventional ECM to HUXMA were 0:1, 1:2, 1:1, 2:1 and 1:0. The results showed that the optical density (OD) of hBMSCs was higher than that of HUVECs, while the coculture with a 1:2 ratio of HUVECs to hBMSCs (4×10^5 hBMSCs, pink column) had similar OD value with hBMSCs cultured alone. As the culture time was prolonged to 48 h, the coculture with a 1:2 ratio of HUVECs to hBMSCs showed the fastest proliferation. Other principles and strategies were also taken into consideration. Firstly, the purpose of this coculture is to induce osteogenesis, and angiogenesis is a crucial and indispensable process, the amounts of hBMSCs for osteogenesis should maintained considerable proportion. Secondly, the viability of HUVECs relied on ECM (especially ECGS in the medium); hence, the concentration of ECGS remained the same as that in the ECM. Thirdly, the proliferation rate of hBMSCs was inhibited under culture conditions with low FBS content (ECM containing 5% FBS, HUXMA containing 10% FBS). Herein, the coculture system with a 1:2 ratio of HUVECs to hBMSCs and a 1:2 ratio of ECM:HUXMA (HUXMA 66% content) was established to ensure an appropriate content of FBS, and the viability of cells in the coculture system substantially increased from 24 h to 48 h.

The cytotoxicity of the selected coculture system was characterized

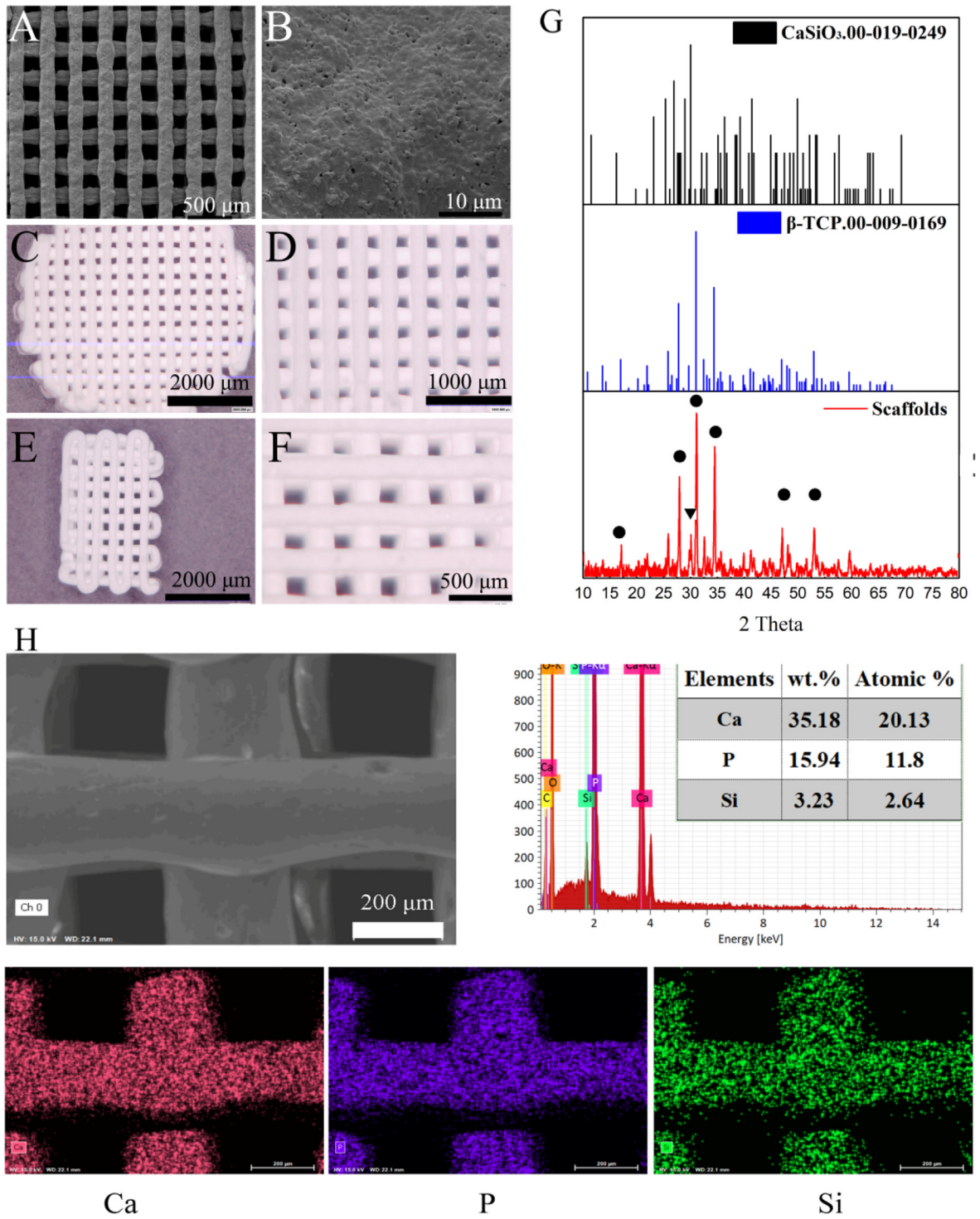

Figure 1. Scaffold morphology (A) SEM image (B) Micro-surface of the scaffolds (C) and (D) 3D microscopy images of the scaffold used for *in vitro* experiments (E) and (F) 3D microscopy images of the scaffold used for submuscular implantation *in vivo* (G) Crystal phase of scaffolds was determined by XRD: ▼ represented $CaSiO_3$ (00-019-0149) characteristic peaks, and • corresponded to β-TCP (00-009-0169) characteristic peaks (H) Elements in the scaffolds were determined by EDS.

by detecting lactate dehydrogenase released from damaged cells, and the results, shown in ESI Fig. 1, indicated that the cytotoxicity of the coculture system could be negligible.

3.3. Cell adhesion and real-time tracking on scaffolds

Based on the optical observation shown in Fig. 3A, the outline of HUVECs resembled cobblestone, while the larger hBMSCs were shaped like shuttles. The HUVECs and hBMSCs were arranged in an island chain-like array at an early stage and ultimately coalesced as a film when cultured *in vitro*. In addition, cell labelling and immunofluorescence were used to evaluate the cell distribution and preliminarily examine protein secretion in the coculture system. As shown in the cell-tracking results in Fig. 3C, cocultured cells initially adhered to the matrix and tended to cluster with other cells of the same type. Cell adhesion was observed after 12 h of culture, and clear communities were observed after 24 h of

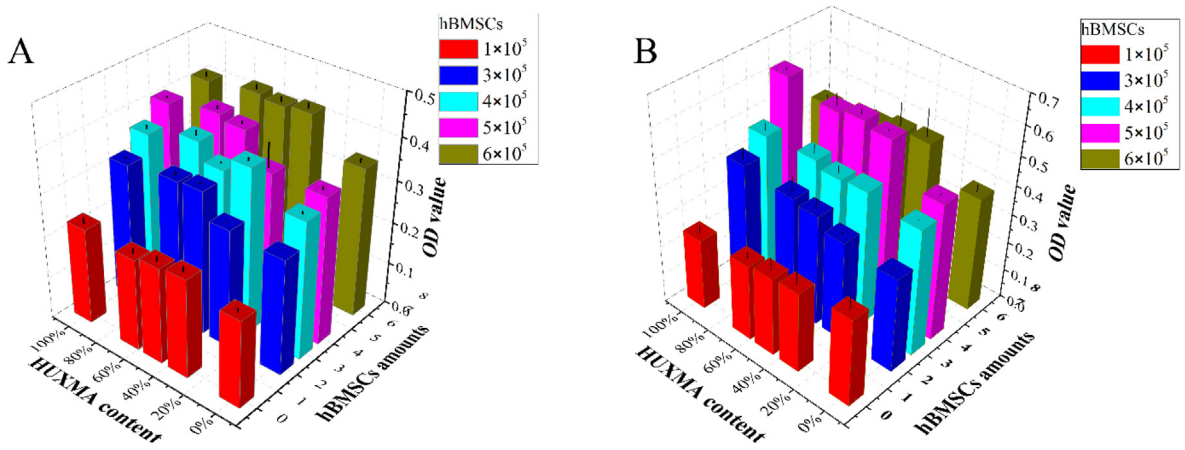

Figure 2. Cell viability of coculture system under different cell and medium proportions after 24 h (A) and 48 h (B). The number of hBMSCs was 0 (red column), 2 × 10^5 (blue column), 3 × 10^5 (cyan column), 4 × 10^5 (pink column), and 6 × 10^5 (brown column), and the corresponding proportions of hBMSCs to HUVECs were 0:1 (0%), 1:2 (33%), 1:1 (50%), 2:1 (66%) and 1:0 (100%). The HUXMA contents were 0%, 33%, 50%, 66% and 100%, and the proportions of conventional ECM to HUXMA were 0:1, 1:2, 1:1, 2:1 and 1:0. (For interpretation of the references to colour in this figure legend, the reader is referred to the Web version of this article.)

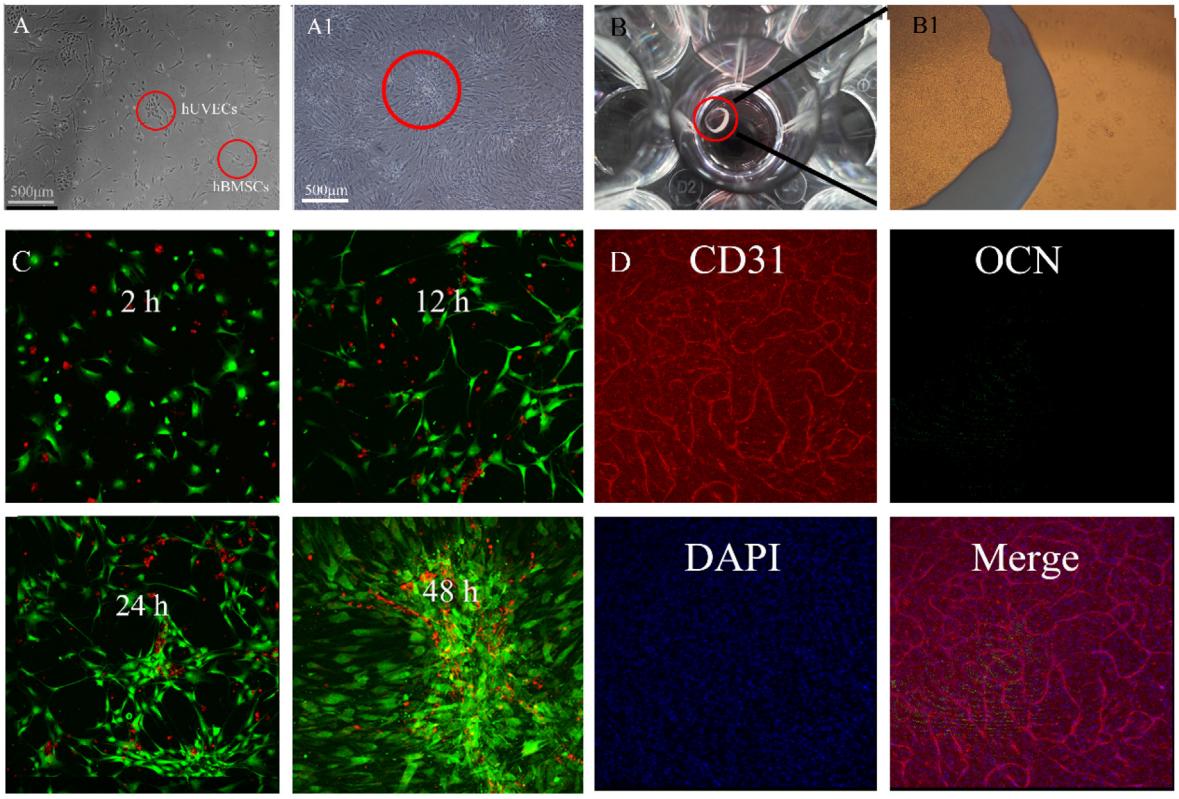

Figure 3. Coculture in a T25 culture plate for 12 h (A) and 72 h (A1). Cells (6 × 10^5) after 7 d of culture in a 24-well culture plate (B) (B1) showed a magnified view (C) Location of HUVECs and hBMSCs on the plate. HUVECs and hBMSCs were indicated by red and green fluorescence, respectively, and the real-time tracking videos were provided in ESI Video 1 and Video 2. (D) Immunofluorescence of HUVECs and hBMSCs cultured on plates. CD31, OCN and cell nuclei were stained. (For interpretation of the references to colour in this figure legend, the reader is referred to the Web version of this article.)

cultivation. Ultimately, the cells were arranged in island chain-like arrays, with HUVECs surrounded by hBMSCs. When the cells were cultured on plates for 7 d, HUVECs secreted PCAM-1 (also known as CD31), which formed a string, hBMSCs showed marked proliferation but little OCN secretion as shown in Fig. 3D.

When cells were seeded on the 3D-printed scaffolds, they could form a film on the surface, as shown in ESI Fig. 2, and could migrate between the extruded fibres. The results of the real-time tracking of HUVECs and hBMSCs on the scaffold were shown in Fig. 4A, and complete videos were provided in ESI Videos 3 and 4. HUVECs and hBMSCs were indicated by red and green fluorescence. hBMSCs were cultured on the scaffold first, as they could adhere to and spread on the scaffold; then, HUVECs were cultured and seemed to be recruited by the hBMSCs, as shown in ESI Video 3.

3.4. Expression of osteogenic differentiation and angiogenic genes in vitro

The expression levels of genes related to osteogenesis and

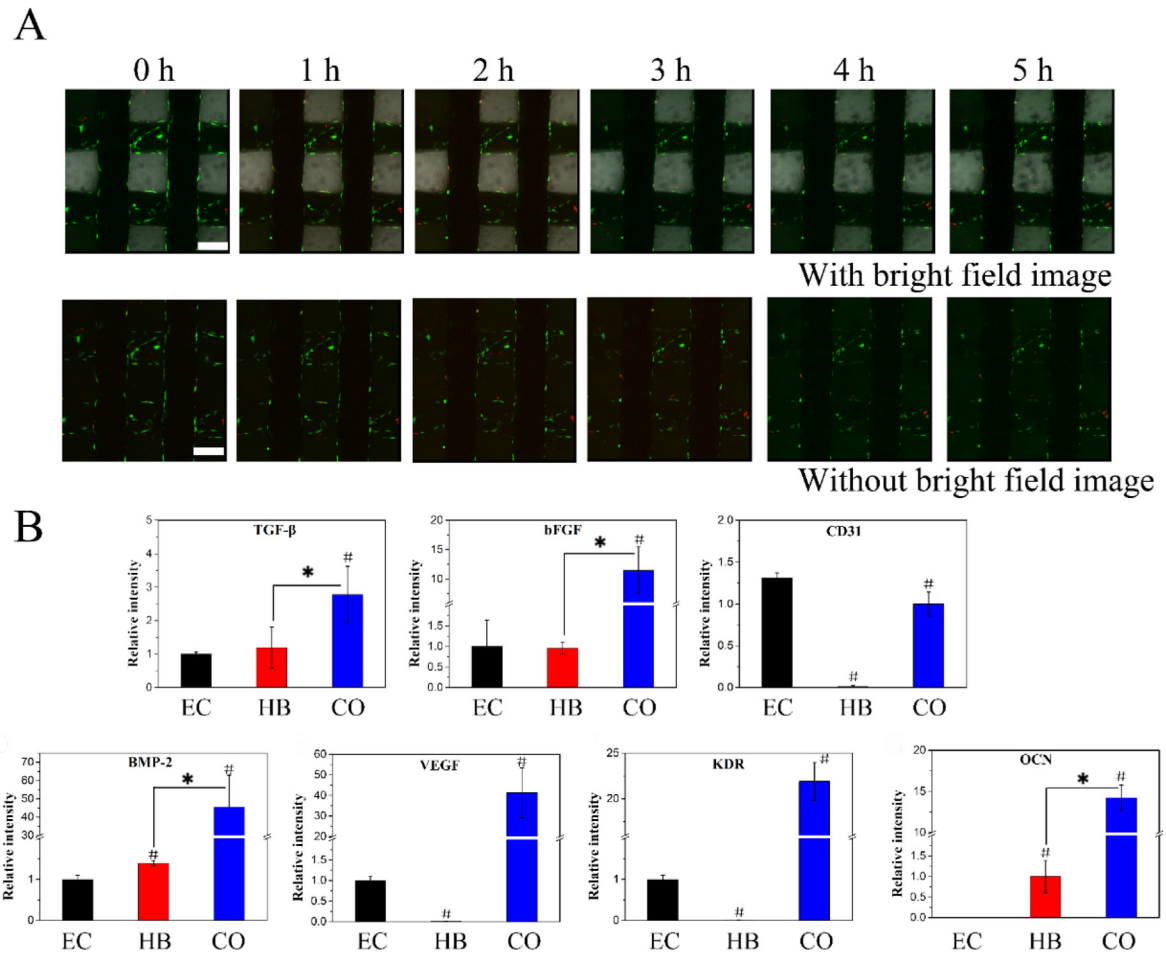

Figure 4. (A) Tracking of HUVECs and hBMSCs on the scaffold. HUVECs and hBMSCs were indicated by red and green fluorescence. hBMSCs were cultured on the scaffold for 12 h, and then HUVECs were added. The observations was carried out after incubating HUVECs for 0-5 h; the scale bar was 200 μm (B) RT-PCR of HUVECs and hBMSCs on the scaffold. Relative gene expression levels of the angiogenic markers TGF-β, bFGF, CD31, BMP2, VEGF, KDR and OCN. (For interpretation of the references to colour in this figure legend, the reader is referred to the Web version of this article.)

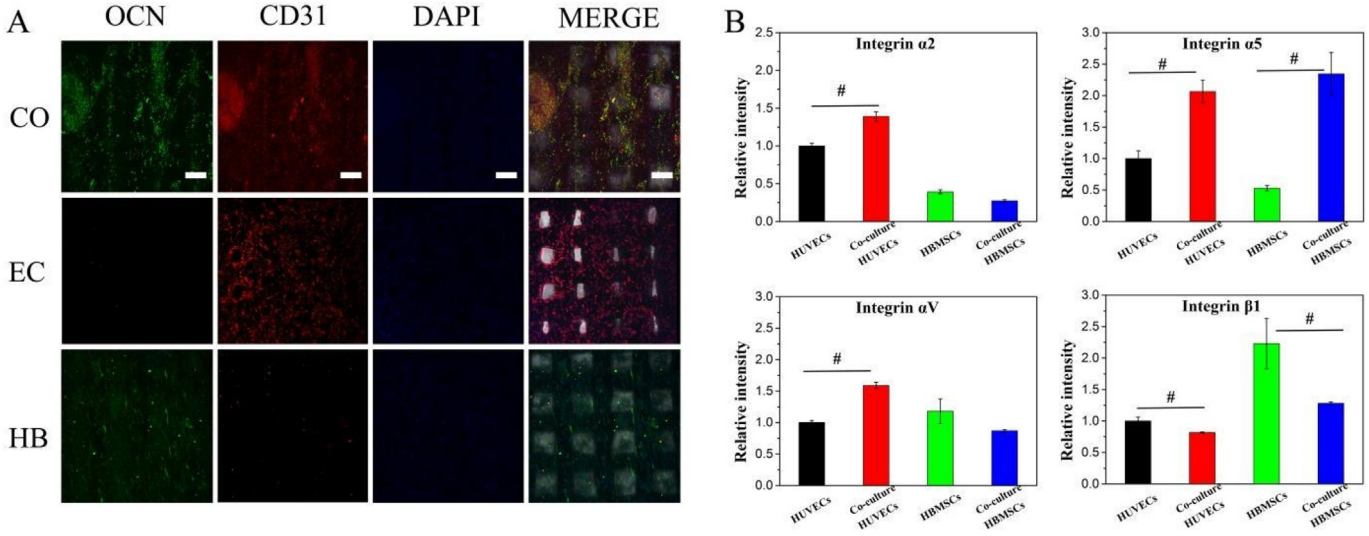

Figure 5. (A) Immunofluorescence of cocultured cells on scaffolds. OCN was labelled with green dye; the red dye represented CD31; and DAPI was used to stain the nuclei. CO, EC and HB represented the cocultured cells, monocultured hBMSCs and monocultured HUVECs, respectively. The scale bar was 200 μm (B) Gene expression levels of integrin subunits α_2, α_5, α_v and β_1 after 12 h of culture. Before extracting RNA, Dynabeads (Dynabeads™ CD31 Endothelial Cell 11155D, Life, USA) was utilized to isolate hBMSCs and HUVECs. (For interpretation of the references to colour in this figure legend, the reader is referred to the Web version of this article.)

angiogenesis were examined via RT-PCR. The group of HUVECs/hBMSCs cocultured on scaffolds was named CO group. The control groups consisted of hBMSCs cultured on scaffolds (named HB group) and HUVECs cultured on scaffolds ((named EC group). The tested gene markers were bFGF, OCN, BMP2, PECAM-1 (CD31), eNOS, KDR (VEGF-R2), TGF-β and VEGF. No significant difference in the bFGF or TGF-β level was observed between the EC and HB groups; however, compared with the other groups, the CO group showed notably upregulated gene expression. VEGF and its receptor KDR were also markedly upregulated in the CO group compared with the EC group, but these genes were not expressed in the HB group. Low CD31 expression was detected in the HB group, and the CD31 expression level in the EC group was higher than that in the CO group. Regarding the osteogenic gene markers BMP2 and OCN, there was no significant difference in the expression of BMP2 between the EC and HB groups, while the CO group showed greatly upregulated BMP2 gene expression. The OCN gene expression level in the CO group was upregulated much more than that in the HB group, and there was no OCN expression in the EC group.

To complement the gene expression level analysis, OCN and CD31 protein secretions were examined via immunofluorescence staining (Fig. 5A). The results were consistent with the RT-PCR results. Notable fluorescence corresponding to secreted OCN was observed in the CO group, while weak fluorescence was observed in the HB group, and no fluorescence was observed in the EC group. The red fluorescence clearly indicated that CD31 was secreted in the CO and EC groups, while trace amounts of CD31 were secreted in the HB group, which might be attributed to the stimulation of hBMSCs by the scaffolds.

The gene expression levels of the integrin subunits α_2, α_5, α_v and β_1 were quantitatively measured, as shown in Fig. 5B. The cocultured cells were isolated via Dynabeads, and then the integrin expression levels were compared. The gene expression levels of integrin α_2, α_5 and α_v were upregulated in HUVECs, while the gene expression of integrin α_5 was upregulated in hBMSCs. This finding indicated that HUVECs adhesion was improved with the establishment of the coculture system. Notably, integrin α_5 expression was upregulated in both hBMSCs and HUVECs, while integrin β_1 expression was downregulated in the coculture compared to the monocultures.

3.5. Osteogenesis and angiogenesis in vivo

The fabricated scaffolds were cultured with cells *in vitro* for 7 d beforehand and then implanted into female nude rats. The cocultured cells formed a film on the scaffold (ESI Fig. 3A). The extent of early osteogenesis and angiogenesis after 2 weeks implantation was measured through H&E and Masson's trichrome staining combined with CD31 and OCN immunohistochemical staining. Little mineralized bone matrix was observed in the EC and HB groups, and secreted collagen I was rare on these scaffolds. Although more collagen I was present on the scaffolds in the CO group than that in the other groups based on Masson's trichrome staining (Fig. 6A2), new bone matrix was not observed by H&E staining. These results suggested that the tissue engineering scaffolds with cocultured cells could induce early collagen secretion and capillary tube formation; however, no mature bone formation was observed.

CD31 immunohistochemical staining revealed signs of lumens or capillary tubes on the scaffolds, which confirmed CD31 secretion in the CO group. Semiquantitative analyses were the average OD calculated by the ratio of the integrated OD to the stained area (Fig. 7D and E). This revealed that the CO group had the ability to quickly form vessels while erythrocytes could gather and form vessel-like structures without a large amount of CD31 protein in the HB and EC groups. Immunohistochemical staining revealed that the area of OCN staining was larger and that average OD was more intense than that of CD31. Although the stained area was widespread in the monoculture and coculture groups, the average OD was more intense in the CO group than in the EC and HB groups, which corresponded with the H&E and Masson staining results. The tendency towards osteogenesis/angiogenesis was more obvious in the CO group than in the EC and HB groups. In summary, tissue engineering scaffolds with cocultured cells could induce early protein secretion (Col-I, CD31 and OCN) and the generation of capillary tubes that secreted CD31. In addition, after 4 and 8 weeks, the scaffolds seemed to degrade, and signs of osteogenesis and angiogenesis became blurred after 4 (ESI Figs. 4) and 8 (ESI Fig. 5) weeks. These observations might be the result of incompatibilities between the nonhomologous seed cells and host cells.

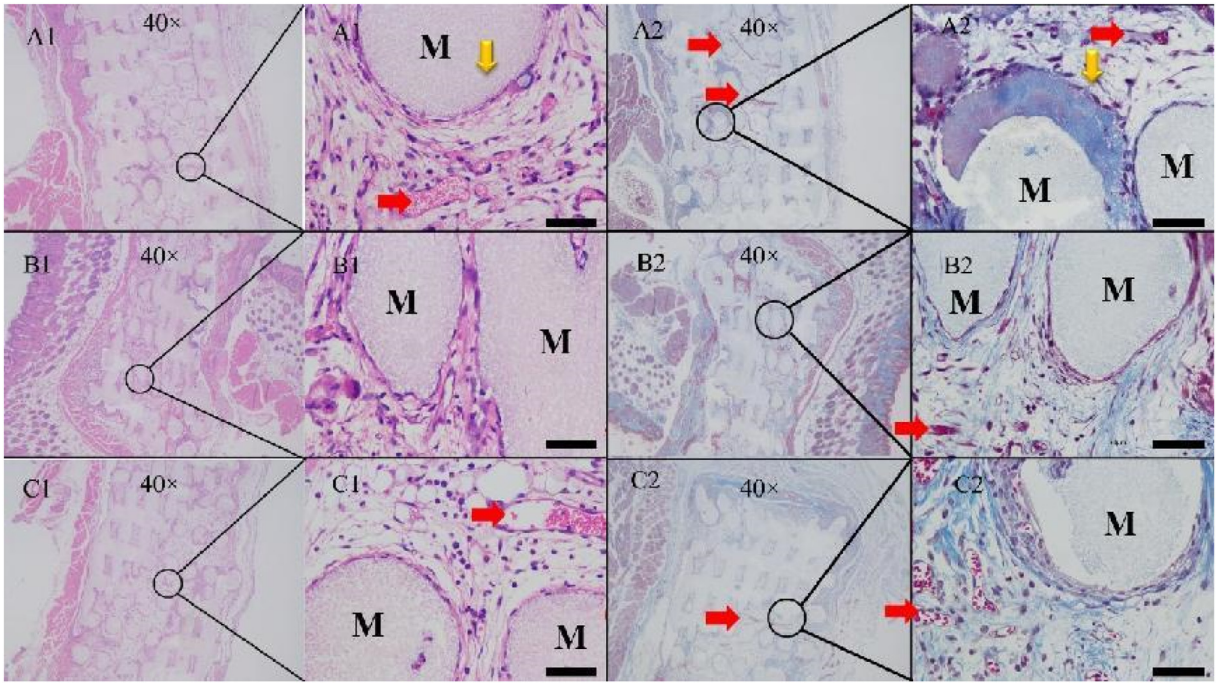

Figure 6. (A–C) Pathological sections from the CO, EC and HB groups after 2 weeks submuscular implantation. The numbers 1 and 2 represented H&E and Masson staining, respectively. The scale bar was 50 μm.

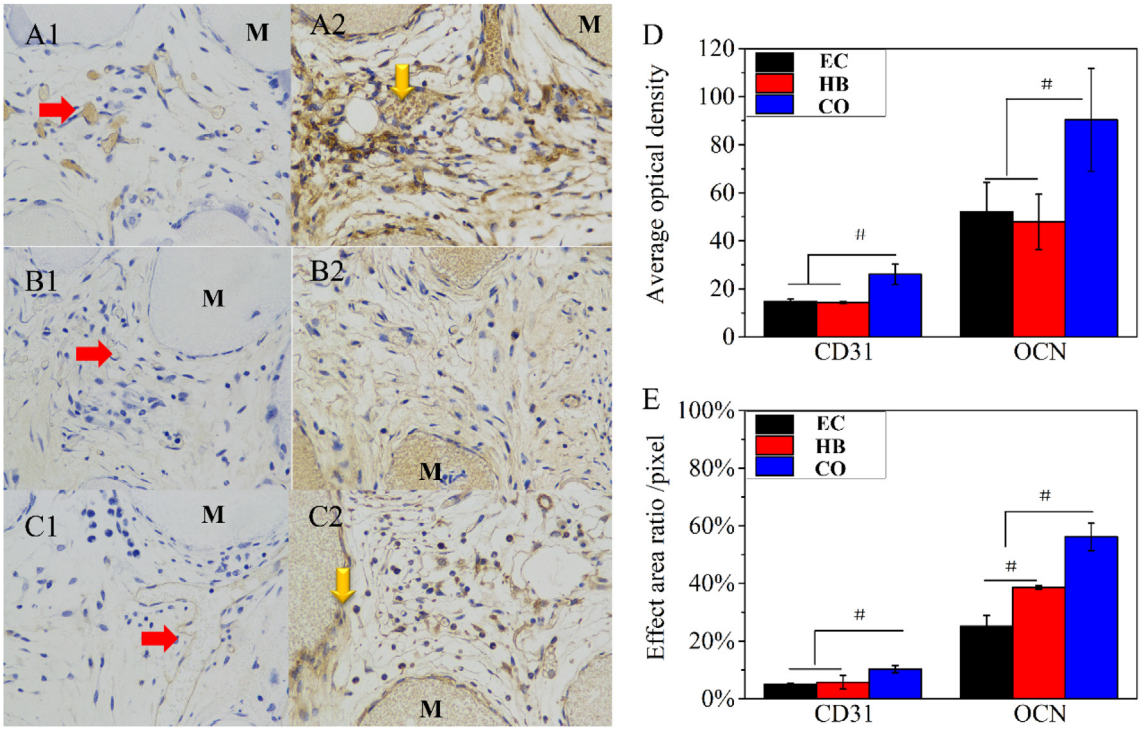

Figure 7. (A–C) Results of immunohistochemical staining in the CO, EC and HB groups after 2 weeks submuscular implantation. The numbers 1 and 2 represented CD31 and OCN staining, respectively. (D) was the average OD values calculated by the ratio of the integrated OD value to the stained area. (E) was the stained area proportion, and the scale bar was 50 μm.

4. Discussion

Angiogenesis and osteogenesis are indispensable for bone regeneration and remain challenges [4]. Traditional tissue engineering approaches utilize exogenous growth factors that can induce osteogenesis but might cause side effects [3]. The scaffolds for cell culture were 3D printed bioactive ceramic scaffolds consisting of β-TCP and $CaSiO_3$, as described in our previous study [26]; this scaffold substrate can be biodegradable, and silicate has been proven to be capable of inducing angiogenesis by upregulating nitric oxide synthase [31] and osteogenesis [6,8]. In addition, the structure of the scaffolds consisted of interconnected pores to facilitate tissue ingrowth.

In this work, a coculture system containing endothelial cells and BMSCs was established to promote osteogenesis and angiogenesis. Moreover, the coculture system resembles that *in vivo* [16]. Initially, the cell and medium ratios needed for the coculture system were undetermined [5,8,32,33] due to the materials and intended purpose of the coculture system. Different cells demand different complete media (mainly different volumes of FBS) and additive factors, such as ECGS. Li et al [6] studied coculture system of HUVECs and hBMSCs cultured at a ratio of 2:1 in 1:1 ECM:HUXMA [34], which showed excellent osteogenesis/angiogenesis. Additionally, a study proved that HUVECs and hBMSCs cultured at a 5:1 ratio can form microcapillary-like structures with upregulated gene expression of CD31 and BMP2, while HUVECs and hBMSCs cultured at a 1:5 ratio tended to favour osteogenesis via the upregulation of Runx-2, ALP, OPN and BSP [5]. In addition, to maintain the viability of HUVECs, cocultures are sometimes maintained using ECM (with ECGS additive factors) [32]. In this work, the coculture conditions were selected based on cell viability, and the cocultured cells were more vigorous with a remarkable proliferation rate, when HUVECs and hBMSCs were cultured at a ratio of 1:2 in HUVECs and hBMSCs media at a ratio of 1:2 (Fig. 2). Since HUVECs were cultured under conditions of low FBS, which led to a low hBMSCs proliferation rate, the content of FBS should be moderate. Additionally, the purpose of this coculture is to promote osteogenesis, and angiogenesis is a crucial and indispensable procedure; hence, the coculture system used a 1:2 ratio of HUVECs and HBMSCs and a 1:2 ratio of HUVECs and hBMSCs medium. In addition, factors added to the ECM (e.g., ECGS) are important for the proliferation of HUVECs; therefore, the content of ECGS in the medium for the coculture system remained the same as that in the ECM. The *in vitro* observations showed that the cells in the establised coculture system tended to aggregate in island chain-like arrays and formed cell–cell films (Fig. 3), the process of which could be finished within 2 d. The HUVECs seemed to be recruited by the hBMSCs, as observed by real-time cell tracking, and the integrin expression of the HUVECs was upregulated. Considerable CD31 was secreted and connected linearly. Furthermore, the *in vivo* studies showed that cell–cell films formed on the 3D scaffolds.

Analysis of the expression levels of osteogenic and angiogenic genes indicated that the coculture system favoured both angiogenesis and osteogenesis. VEGF is a key growth factor in angiogenesis that can mediate the proliferation, migration and differentiation of endothelial cells and induce endothelial cell blood vessel sprouting and cavity formation [12]. Its receptor, KDR, also known as VEGF-R2, plays a role in regulating lymphatic and vascular endothelial cells [6]. The expression of these genes was far more upregulated in the coculture system than in the monocultures in our study. bFGF is another multifunctional factor in the early stage of angiogenesis that can regulate the proliferation, migration and differentiation of endothelial cells and promote the formation of capillaries [12]. TGF-β is known as an important cytokine in the process of bone formation that regulates the release of VEGF and bFGF; Additionally, it is a chemotactic factor involved in the recruitment and proliferation of peripheral mesenchymal cells [14]. bFGF and TGF-β gene expression was far more upregulated in the CO group than in the EC and HB groups, with no significant variation between the EC and HB groups. CD31 (PECAM-1) is a widely investigated protein involved in angiogenesis that regulates endothelial cell adhesion and participates in endothelial cell migration, angiogenesis and integrin activation [35,36]. In our study, CD31 gene expression was upregulated in the EC group

compared with the CO group, which was attributed to the presence of RNA from hBMSCs. Regarding osteogenic gene markers [37], BMP2 is also a widespread growth factor belonging to the TGF-β superfamily and has been proven to efficiently promote osteogenesis [38]. In our study, BMP2 gene expression was far more upregulated in the CO group than that in the EC and HB groups, while BMP2 gene expression was higher in the HB group than in the EC group. The late-stage osteogenic marker OCN is associated with bone mineralization [39,40]. OCN gene expression was also far more upregulated in the CO group than in the EC and HB groups, but OCN was not expressed in the EC group.

As a complement to the analysis of gene expression at the transcript level, the levels of CD31 and OCN protein secretion were analysed through immunofluorescence. The tendency of OCN secretion was consistent with the RT-PCR results. The fluorescence intensity of OCN in the CO group was much stronger than that in the HB group, while no secreted OCN was detected in the EC group. CD31 fluorescence in the CO and EC groups was much more intenser than that in the HB group. Nevertheless, it is worth mentioning that weak CD31 fluorescence was observed in the HB group, which indicated the induction of angiogenesis by the scaffolds. These results indicated that both osteogenesis and angiogenesis were promoted by the coculture of HUVECs and hBMSCs on the 3D-printed bioactive ceramic scaffolds.

An *in vivo* study was performed with submuscular implants in nude rats. The submuscular region of the biceps femoris could favour osteogenesis because of the large number of cells and high blood supply [41]. In the early stage, although little new bone matrix was observed, the capillary tube formation and protein secretion upregulation were confirmed with the coculture system (Fig. 6). However, protein secretion decreased over prolonged time periods. At 4 and 8 weeks, the harvested implants showed only some blurred OCN staining without signs of CD31 staining (ESI Figs. 4 and 5). The reasons for the lack of ectopic bone formation might be related to species differences between the seed and host cells. MSCs have been reported to recruit pericytes instead of functioning as stem cells [11]; thus, seed cells might be able to recruit pericytes while host cells support tissue regeneration. The seed cells on the scaffolds could recruit pericytes and promote osteogenic protein secretion but the protein secretion were subject to the ectopic microenvironment and the species differences between the seed and host cells. As a result, little new bone matrix deposition was observed in the nude rats, but osteogenic protein secretion (Col-1, OCN), angiogenic protein secretion (CD31) and capillary tube formation were observed early after implantation.

Additionally, it should be noted that bone regeneration is a complex and long-term process that comprises multiple components, such as osteogenesis, angiogenesis, and osteoimmunology, which are regulated by the physicochemical and mechanical microenvironment [42,43]. Bone healing and cell fate can be controlled by physicochemical and mechanical stimuli, especially under 3D conditions [44]. This work confirmed the osteogenic and angiogenic effects of the obtained 3D-printed bioceramic scaffolds and coculture system and demonstrated several advantages of clinical translation [45,46]. However, the underlying mechanisms promoting osteogenesis and angiogenesis require further investigation. A systematic exploration is also required to reveal how physicochemical and mechanical cues are recognized by cells and mediate cell fate under the conditions of HUVECs/hBMSCs coculture and then screen for the crucial molecular events [47] and cytokines [48,49]. In addition, in cocultures of cells from different species, the regulatory effects of biomaterials on the cells and the mechanisms underlying these effects might be more complicated compared to those in traditional *in vitro* monocultures. In coculture systems, the related signalling pathways might be cascades of osteogenic/angiogenic pathways, and the involved cytokines could be more diverse. Hence, further studies are needed to discover how physicochemical and mechanical cues can be recognized by cocultured cells and mediate the synergistic coupling of osteogenesis/angiogenesis.

5. Conclusions

In the present study, potential tissue engineering scaffolds for bone regeneration without exogenous growth factors were constructed. The 3D-printed bioactive ceramic scaffolds were composed of β-TCP and $CaSiO_3$. A coculture system consisting of HUVECs and hBMSCs was utilized to promote angiogenesis and osteogenesis after identifying the appropriate cell and medium proportions. The resulting coculture system showed negligible cytotoxicity, and cells gathered into island chain-like arrays on the scaffolds *in vitro*. HUVECs formed CD31 strings *in vitro*, and the presence of hBMSCs favoured cell adhesion of HUVECs. The bone tissue engineering scaffolds, with an appropriate proportion of HUVECs/hBMSCs cultured onto 3D-printed bioactive ceramic scaffolds, promoted the expression of genes related to osteogenesis and angiogenesis *in vitro*. In addition, protein secretion (OCN, CD31 and Col-I) and capillary tube formation were observed during the initial period after implantation of the bone tissue engineering scaffolds in the submuscular region *in vivo*. Thus, this 3D-printed bioceramic scaffold and coculture system has potential as a candidate for bone tissue engineering applications.

Credit author statement

Xiao Liu: Conceptualization, Methodology, Investigation, Writing-original draft, Data curation. Naru zhao: Methodology, Investigation, Writing-review&editing. Haifeng Liang: Investigation (*in vivo*), Writing-review&editing. Bizhi Tan: Writing-review&editing. Fangli Huang: Writing-review&editing. Hao Hu: Writing-review&editing. Yan Chen: Writing-review&editing. Gang Wang: Writing-review&editing. Zemin Ling: Writing-review&editing. Chun Liu: Writing-review&editing. Yali Miao: Conceptualization, Resources, Writing-review&editing. Yingjun Wang: Conceptualization, Resources, Writing-review&editing. Xuenong Zou: Conceptualization, Writing-review&editing, Supervision, Funding acquisition, Project administration.

Data availability

The data used in the present study are available from the corresponding author on reasonable request.

Declaration of competing interest

The authors declare that they have no known competing financial interests or personal relationships that could have appeared to influence the work reported in this paper.

Acknowledgements

This work was financially supported by the National Natural Science Foundation of China (52202358, 32071341, 32101062, 52003302), GuangDong Basic and Applied Basic Research Foundation (2021A1515110824, 2022A1515012607, 2019A1515110005), National Key Research and Development Plan (2017YFC1105000, 2017YFA0205600), and Science and Technology Program of Guangdong Province (2019B010941002).

Appendix A. Supplementary data

Supplementary data to this article can be found online at https://doi.org/10.1016/j.jot.2022.10.008.

References

[1] Burg KJ, Porter S, Kellam JF. Biomaterial developments for bone tissue engineering. Biomaterials 2000;21(23):2347–59.
[2] Tayalia P, Mooney DJ. Controlled growth factor delivery for tissue engineering. Adv Mater 2009;21(32–33):3269–85.

[3] Yuan H, Fernandes H, Habibovic P, de Boer J, Barradas AM, de Ruiter A, et al. Osteoinductive ceramics as a synthetic alternative to autologous bone grafting. Proc Natl Acad Sci USA 2010;107(31):13614–9.
[4] LeGeros RZ. Calcium phosphate-based osteoinductive materials. Chem Rev 2008; 108(11):4742–53.
[5] Kang Y, Kim S, Fahrenholtz M, Khademhosseini A, Yang Y. Osteogenic and angiogenic potentials of monocultured and co-cultured human-bone-marrow-derived mesenchymal stem cells and human-umbilical-vein endothelial cells on three-dimensional porous beta-tricalcium phosphate scaffold. Acta Biomater 2013; 9(1):4906–15.
[6] Li H, Xue K, Kong N, Liu K, Chang J. Silicate bioceramics enhanced vascularization and osteogenesis through stimulating interactions between endothelia cells and bone marrow stromal cells. Biomaterials 2014;35(12):3803–18.
[7] He D, Li H. Biomaterials affect cell-cell interactions in vitro in tissue engineering. J Mater Sci Technol 2021;63:62–72.
[8] Deng Y, Jiang C, Li C, Li T, Peng M, Wang J, et al. 3D printed scaffolds of calcium silicate-doped beta-TCP synergize with co-cultured endothelial and stromal cells to promote vascularization and bone formation. Sci Rep 2017;7(1):5588.
[9] Park JW, Fu S, Huang B, Xu RH. Alternative splicing in mesenchymal stem cell differentiation. Stem Cell 2020;38(10):1229–40.
[10] Khatibi S, Kheyrolahzadeh K, Barzegari A, Saadat YR, Vahed SZ. Medicinal signaling cells: a potential antimicrobial drug store. J Cell Physiol 2020;235(1): 7731–46.
[11] Caplan AI. Mesenchymal stem cells: time to change the name. Stem Cells Transl Med 2017;6(6):1445–51.
[12] Rouwkema J, Khademhosseini A. Vascularization and angiogenesis in tissue engineering: beyond creating static networks. Trends Biotechnol 2016;34(9): 733–45.
[13] Malhotra A, Habibovic P. Calcium phosphates and angiogenesis: implications and advances for bone regeneration. Trends Biotechnol 2016;34(12):983–92.
[14] Saran U, Piperni SG, Chatterjee S. Role of angiogenesis in bone repair. Arch Biochem Biophys 2014;561:109–17.
[15] Piard C, Jeyaram A, Liu Y, Caccamese J, Jay SM, Chen Y, et al. 3D printed HUVECs/MSCs cocultures impact cellular interactions and angiogenesis depending on cell-cell distance. Biomaterials 2019;222:119423.
[16] Grellier M, Bordenave L, Amedee J. Cell-to-cell communication between osteogenic and endothelial lineages: implications for tissue engineering. Trends Biotechnol 2009;27(10):562–71.
[17] Kang Y, Kim S, Bishop J, Khademhosseini A, Yang Y. The osteogenic differentiation of human bone marrow MSCs on HUVEC-derived ECM and beta-TCP scaffold. Biomaterials 2012;33(29):6998–7007.
[18] Zehnder T, Boccaccini AR, Detsch R. Biofabrication of a co-culture system in an osteoid-like hydrogel matrix. Biofabrication 2017;9(2):025016.
[19] Essaouiba A, Jellali R, Shinohara M, Scheidecker B, Legallais C, Sakai Y, et al. Analysis of the behavior of 2D monolayers and 3D spheroid human pancreatic beta cells derived from induced pluripotent stem cells in a microfluidic environment. J Biotechnol 2021;330:45–56.
[20] Hsu TW, Lu YJ, Lin YJ, Huang YT, Hsieh LH, Wu BH, et al. Transplantation of 3D MSC/HUVEC spheroids with neuroprotective and proangiogenic potentials ameliorates ischemic stroke brain injury. Biomaterials 2021;272:120765.
[21] Byun H, Jang GN, Lee J, Hong M-H, Shin H, Shin H. Stem cell spheroid engineering with osteoinductive and ROS scavenging nanofibers for bone regeneration. Biofabrication 2021;13(3):034101.
[22] Kelly CN, Wang T, Crowley J, Wills D, Pelletier MH, Westrick ER, et al. High-strength, porous additively manufactured implants with optimized mechanical osseointegration. Biomaterials 2021;279:121206.
[23] Wang C, Huang W, Zhou Y, He L, He Z, Chen Z, et al. 3D printing of bone tissue engineering scaffolds. Bioact Mater 2020;5(1):82–91.
[24] Li Q, Chen T, Liang J, Zhang C, Li J, Zhou Y, et al. Manufacturing of ceramic cores: from hot injection to 3D printing. J Mater Sci Technol 2023;134:95–105.
[25] Jameson JL, Longo DL. Precision medicine–personalized, problematic, and promising. N Engl J Med 2015;372(23):2229–34.
[26] Dong Y, Duan H, Zhao N, Liu X, Ma Y, Shi X. Three-dimensional printing of β-tricalcium phosphate/calcium silicate composite scaffolds for bone tissue engineering. Bio-Des Manuf 2018;1(2):146–56.
[27] Zhou P, Xia D, Ni Z, Ou T, Wang Y, Zhang H, et al. Calcium silicate bioactive ceramics induce osteogenesis through oncostatin M. Bioact Mater 2021;6(3): 810–22.
[28] Diao J, OuYang J, Deng T, Liu X, Feng Y, Zhao N, et al. 3D-plotted beta-tricalcium phosphate scaffolds with smaller pore sizes improve in vivo bone regeneration and biomechanical properties in a critical-sized calvarial defect rat model. Adv Healthc Mater 2018;7(17):e1800441.
[29] Liu X, Zhao N, Duan H, Ma Y, Guo X, Diao J, et al. The effects of dissociated rods and rod-surfaced microspheres on bone mesenchymal stem cellular viability. RSC Adv 2017;7(25):15284–92.
[30] Kreiger M, Matsudaira P, Mastudaira P, Darnel J, Lodish HF, Krieger M, et al. Molecular cell biology. Scientific American Books; 2013. p. 1–17.
[31] Bose S, Fielding G, Tarafder S, Bandyopadhyay A. Understanding of dopant-induced osteogenesis and angiogenesis in calcium phosphate ceramics. Trends Biotechnol 2013;31(10):594–605.
[32] Unger RE, Sartoris A, Peters K, Motta A, Migliaresi C, Kunkel M, et al. Tissue-like self-assembly in cocultures of endothelial cells and osteoblasts and the formation of microcapillary-like structures on three-dimensional porous biomaterials. Biomaterials 2007;28(27):3965–76.
[33] Au P, Tam J, Fukumura D, Jain RK. Bone marrow-derived mesenchymal stem cells facilitate engineering of long-lasting functional vasculature. Blood 2008;111(9): 4551–8.
[34] Li H, Daculsi R, Grellier M, Bareille R, Bourget C, Remy M, et al. The role of vascular actors in two dimensional dialogue of human bone marrow stromal cell and endothelial cell for inducing self-assembled network. PLoS One 2011;6(2):e16767.
[35] Betsholtz C. Vascular biology: transcriptional control of endothelial energy. Nature 2016;529(7585):160–1.
[36] Yancopoulos GD, Davis S, Gale NW, Rudge JS, Wiegand SJ, Holash J. Vascular-specific growth factors and blood vessel formation. Nature 2000;407(6801):242–8.
[37] Tao ZS, Zhou WS, Xu HG, Yang M. Parathyroid hormone (1-34) can reverse the negative effect of valproic acid on the osseointegration of titanium rods in ovariectomized rats. J Orthop Translat 2021;27:67–76.
[38] Lin Z, Shen D, Zhou W, Zheng Y, Kong T, Liu X, et al. Regulation of extracellular bioactive cations in bone tissue microenvironment induces favorable osteoimmune conditions to accelerate in situ bone regeneration. Bioact Mater 2021;6(8): 2315–30.
[39] Li L, Yu M, Li Y, Li Q, Yang H, Zheng M, et al. Synergistic anti-inflammatory and osteogenic n-HA/resveratrol/chitosan composite microspheres for osteoporotic bone regeneration. Bioact Mater 2021;6(5):1255–66.
[40] Geng Z, Li X, Ji L, Li Z, Zhu S, Cui Z, et al. A novel snail-inspired bionic design of titanium with strontium-substituted hydroxyapatite coating for promoting osseointegration. J Mater Sci Technol 2021;79:35–45.
[41] Song G, Habibovic P, Bao C, Hu J, van Blitterswijk CA, Yuan H, et al. The homing of bone marrow MSCs to non-osseous sites for ectopic bone formation induced by osteoinductive calcium phosphate. Biomaterials 2013;34(9):2167–76.
[42] Ghimire S, Miramini S, Richardson M, Mendis P, Zhang L. Role of dynamic loading on early stage of bone fracture healing. Ann Biomed Eng 2018;46(11):1768–84.
[43] Zhang L, Richardson M, Mendis P. Role of chemical and mechanical stimuli in mediating bone fracture healing. Clin Exp Pharmacol Physiol 2012;39(8):706–10.
[44] Ganadhiepan G, Miramini S, Patel M, Mendis P, Zhang L. Bone fracture healing under Ilizarov fixator: influence of fixator configuration, fracture geometry, and loading. Int J Numer Method Biomed Eng 2019;35(6):e3199.
[45] Peng Y, Li J, Lin H, Tian S, Liu S, Pu F, et al. Endogenous repair theory enriches construction strategies for orthopaedic biomaterials: a narrative review. Biomater Translat 2021;2(4):343–60.
[46] Shi Y, He R, Deng X, Shao Z, Deganello D, Yan C, et al. Three-dimensional biofabrication of an aragoniteenriched self-hardening bone graft substitute and assessment of its osteogenicity in vitro and in vivo. Biomater Translat 2020;1(1):13.
[47] Liu Y, Fang J, Zhang Q, Zhang X, Cao Y, Chen W, et al. Wnt10b-overexpressing umbilical cord mesenchymal stem cells promote critical size rat calvarial defect healing by enhanced osteogenesis and VEGF-mediated angiogenesis. J Orthop Translat 2020;23:29–37.
[48] Zhang E, Miramini S, Patel M, Richardson M, Ebeling P, Zhang L. Role of TNF-α in early-stage fracture healing under normal and diabetic conditions. Comput Methods Progr Biomed 2022;213:106536.
[49] Sun X, Li X, Qi H, Hou X, Zhao J, Yuan X, et al. MiR-21 nanocapsules promote early bone repair of osteoporotic fractures by stimulating the osteogenic differentiation of bone marrow mesenchymal stem cells. J Orthop Translat 2020;24:76–87.